9. GREAT-CIRCLE REDUCTIONS

The great-circle reductions combined the observations obtained in a time interval of up to nine hours into a set of one-dimensional coordinates of the objects, the so-called abscissae, defined along a designated reference great circle. These were the main input to the subsequent sphere solution, in which the astrometric parameters of the stars were derived. The great-circle reductions also determined the geometrical instrument parameters, including the basic angle, transforming the observed signal phases into true angles on the sky, and the accurate along-scan attitude needed for the Tycho astrometry. This chapter describes the principles of the great-circle reductions and their practical implementation by FAST and NDAC. Great-circle results obtained by the two reduction consortia are presented. The early results were found to be affected by systematic errors, which however disappeared after several iterations of the great-circle reductions, by using improved star catalogues from previous iterations, fine tuning of the instrument description, and special treatment of star outliers. The final quality of the results was confirmed by intercomparisons between the consortia.

9.1. Introduction

In the Hipparcos great-circle reduction semi-contiguous batches of grid coordinates, each computed from image dissector tube data collected over an observational frame (see Chapter 5), were combined in so-called reference great-circle sets and processed together. A reference great-circle set contained the data collected over one orbit of the satellite and generally covered 2 to 4 revolutions, or 4 to 9 hours of data. All such data were referred to a reference frame, corresponding to a great circle chosen somewhere in the middle of the band on the celestial sphere scanned during the reference great-circle set. The abscissae of the stars contained in the reference great-circle set and an improved along-scan attitude were computed in this intermediate reference frame, together with instrument parameters, by a least-squares adjustment.

Data obtained from the Hipparcos main grid provided along-scan information only. Therefore, and because of the small inclination of the scanning circles with respect to the reference great circle, the great-circle reduction could only determine one component of the star position and spacecraft attitude in the reference great-circle frame: the star abscissa v along the reference great circle and the along-scan attitude ψ. The star ordinate r and the two transverse attitude components θ and ϕ could not be estimated. Hence they did not participate in the least-squares adjustment, but were used as obtained

from the attitude reconstruction results (see Chapter 7), using the (updated) Input Catalogue. No effort was made at this stage to estimate the proper motions and parallax: they could not be estimated due to the very limited time span of the reference great-circle sets. The final great-circle reductions were all carried out with respect to a star catalogue based on preliminary reductions of all the Hipparcos data, providing stellar coordinates with errors that were negligible for the purpose of the great-circle reduction process.

9.2. Great-Circle Reduction

The great-circle reduction forms a geometric adjustment problem on the sphere with grid coordinates as observations. Semi-contiguous batches of up to 70 000 grid coordinates, gathered during about 2–4 revolutions, were processed together, producing one observation equation for each grid coordinate. The observation equations were solved by a least-squares adjustment with a diagonal weight matrix for the grid coordinates. The unknown parameters were roughly 1800 star abscissae, forming our prime objective, up to 15 000 along-scan attitude parameters, and some 24 instrumental parameters. In fact two types of along-scan reconstructed attitude were produced. At first a geometric along-scan attitude was estimated, consisting of one parameter for each observational frame of 2.133 ... s. Later the attitude was smoothed to form a continuous representation using about 500 B-splines (one every $\simeq$ 2 minutes). Smoothing of the attitude also improved the quality of the star abscissae, although excessive smoothing could introduce systematic errors. This was verified by statistical tests; when necessary, the number of B-splines, and the location of knots, were adjusted.

Observation Equations

The geometric direction to a star in the reference great-circle frame at set mid-time was expressed by two angles v (abscissa) and r (ordinate). The determination of the abscissae v were the prime objective of the great-circle reduction. The abscissa–ordinate pair (v_i, r_i) for star number i was related to the grid coordinate G_{ik} observed for the star in frame number k, in three steps. First, (v_i, r_i) were transformed into the apparent (or 'proper') star direction at the time of observation, expressed either in the celestial reference frame (Section 12.3) or directly in the reference great-circle frame (Section 11.2), using the known orientation of the reference great circle. Secondly, the direction to the star was transformed into the instrument reference frame, yielding the field angles (η_{ik}, ζ_{ik}) or field coordinates (w_{ik}, z_{ik}), as defined in Section 10.2. Thirdly, the field angles or field coordinates were related to the observations G_{ik} which were defined with respect to the modulating grid by means of the field-to-grid transformation, described by the instrument parameters (Section 10.2).

The transformation of the reference great-circle frame into the reference frame linked to the instrument was described by the three angles $(\psi_k, \theta_k, \phi_k)$ corresponding to the spacecraft attitude. The angles θ_k and ϕ_k were rotations around the y and x axes of the instrument, and specified the direction of the z axis. The angle ψ_k specified the orientation of the instrument around the z axis. The notation used here for these angles corresponds to that used in the FAST attitude model (Equation 7.23), but the presentation below is valid for any representation of the attitude in which (θ_k, ϕ_k) describe the 'transverse attitude' (in NDAC given by the heliotropic angles ξ and ν;

see Section 7.3) and ψ_k describes the 'along-scan attitude' (in NDAC given by the heliotropic angle Ω).

The transformation from field coordinates to grid coordinates, including corrections to the basic angle, is described in Chapter 10 (see also Volume 2, Chapter 10). It usually required 24 or more instrument parameters, which for notational convenience are collected in a vector $\mathbf{d}$ (see Section 9.6).

The relation between the grid coordinate and geometric position was written symbolically as:

$$G_{ik} = G(\nu_i, r_i, \psi_k, \theta_k, \phi_k, \mathbf{d}, \ldots) + \epsilon'_{ik} \qquad [9.1]$$

with ϵ'_{ik} representing the photon noise effect on the grid coordinates. The parameters needed to correct for aberration, relativistic effects, residual proper motion and parallax are not mentioned explicitly in the equations. More details about these computations can be found in Chapter 12.

Linear observation equations, needed for the least-squares estimation, were obtained by taking the truncated Taylor expansion of Equation 9.1 in a point G_{ik}^{calc} calculated from a provisional star catalogue, star mapper attitude and instrument calibration. The linearized equation is:

$$\begin{aligned}\Delta G_{ik} = {} & \frac{\partial G_{ik}}{\partial \nu_i}\Delta\nu_i + \frac{\partial G_{ik}}{\partial \psi_k}\Delta\psi_k + \frac{\partial G_{ik}}{\partial \mathbf{d}'}\Delta\mathbf{d} + \frac{\partial G_{ik}}{\partial r_i}\Delta r_i \\ & + \frac{\partial G_{ik}}{\partial \theta_k}\Delta\theta_k + \frac{\partial G_{ik}}{\partial \phi_k}\Delta\phi_k + \ldots + O(\Delta^2) + \epsilon'_{ik}\end{aligned} \qquad [9.2]$$

with $\Delta G_{ik} = G_{ik}^{\mathrm{obs}} - G_{ik}^{\mathrm{calc}}$. The Δ-quantities on the right hand side were the unknown corrections to the provisional, or approximate, values for the parameters used in the calculation of G_{ik}^{calc}. The term $O(\Delta^2)$ represents the linearization error, which is of second order in the corrections. When the grid coordinates were expressed in angular units (radians), the partial derivatives with respect to ν_i and ψ_k were close to -1 and $+1$ respectively. The partial derivatives in r_i, θ_k and ϕ_k were much smaller in absolute value ($\lesssim 10^{-2}$), but not zero. The reason is that the grid coordinates G only referred to the along-scan component, while the other component H was not measured, so that information on the star ordinate and the transverse attitude components was only available through the inclination of the scan circles with respect to the reference great circle. This inclination was at most about $\pm 1\overset{\circ}{.}5$ through the choice of the reference great circle close to the mean scanning direction in the data set.

Therefore, only the corrections $\Delta\nu_i$, $\Delta\psi_k$ and $\Delta\mathbf{d}$ were computed during the least-squares adjustment; no attempt was made to estimate Δr_i, $\Delta\theta_k$ and $\Delta\phi_k$ in the great-circle reduction. The observation equations were consequently reduced to:

$$\Delta G_{ik} = \frac{\partial G_{ik}}{\partial \nu_i}\Delta\nu_i + \frac{\partial G_{ik}}{\partial \psi_k}\Delta\psi_k + \frac{\partial G_{ik}}{\partial \mathbf{d}'}\Delta\mathbf{d} + \epsilon_{ik} \qquad [9.3]$$

In this equation ϵ_{ik} is a general noise term including:

(1) the photon noise error ϵ'_{ik};

(2) the projection error on the reference great circle:

$$\epsilon''_{ik} = \frac{\partial G_{ik}}{\partial r_i}\Delta r_i + \frac{\partial G_{ik}}{\partial \theta_k}\Delta\theta_k + \frac{\partial G_{ik}}{\partial \phi_k}\Delta\phi_k \qquad [9.4]$$

(3) various modelling errors (e.g. instrument, attitude, residual proper motion and parallax);

(4) the linearization error $O(\Delta^2)$.

The first component is the most important. At the great-circle level it could be modelled as Gaussian noise.

Least-Squares Solution

The observed grid coordinate differences ΔG_{ik} were collected in a vector $\mathbf{y}$ of length m, and the unknown corrections in a vector $\mathbf{x}$ of length n. Equation 9.3 could thus be written in matrix notation as:

$$\begin{aligned} \mathbf{y} &= \mathbf{A}\,\mathbf{x} + \mathbf{e} \\ &= \mathbf{A}_\mathrm{S}\mathbf{x}_\mathrm{S} + \mathbf{A}_\mathrm{A}\mathbf{x}_\mathrm{A} + \mathbf{A}_\mathrm{I}\mathbf{x}_\mathrm{I} + \mathbf{e} \end{aligned} \qquad [9.5]$$

with the $m \times n$ design matrix $\mathbf{A}$ of partial derivatives. This system of equations was partitioned in a star part, an attitude part and an instrument part, denoted respectively by suffix S, A and I in Equation 9.5. The sub-matrices $\mathbf{A}_\mathrm{A}$ and $\mathbf{A}_\mathrm{S}$ were very sparse, each of them containing only one non-zero element per row. $\mathbf{A}_\mathrm{I}$ on the other hand was almost completely filled.

Although Equation 9.5 had many solutions, it was not difficult to select a unique solution, $\hat{\mathbf{x}}$, namely one for which $\mathbf{A}\,\hat{\mathbf{x}}$ was as close as possible to the observed data $\mathbf{y}$. The well-known least-squares solution follows from minimising the residual sum of squares $E = \hat{\mathbf{e}}'\mathbf{Q}_y^{-1}\hat{\mathbf{e}}$, with $\hat{\mathbf{e}} = \mathbf{y} - \mathbf{A}\,\hat{\mathbf{x}}$ the vector of least-squares residuals, and $\mathbf{Q}_y$ the covariance matrix of the observations $\mathbf{y}$. The least-squares solution $\hat{\mathbf{x}}$ was computed by solving the normal equations:

$$(\mathbf{A}'\mathbf{Q}_y^{-1}\mathbf{A})\,\hat{\mathbf{x}} = \mathbf{A}'\mathbf{Q}_y^{-1}\mathbf{y} \qquad [9.6]$$

It deserves to be emphasized that the vector of observations $\mathbf{y}$ was, from a statistical viewpoint, a stochastic variable; consequently the least-squares estimate $\hat{\mathbf{x}}$, the residuals $\hat{\mathbf{e}}$, and other functions of these variables, such as E, were also stochastic. The errors in the observations were dominated by photon noise, and could therefore be assumed to be uncorrelated. Consequently a simple diagonal covariance matrix $\mathbf{Q}_y$ could be used.

The least-squares solution was computed using Cholesky factorization of the square symmetric (semi-)positive definite normal matrix $\mathbf{A}'\mathbf{Q}_y^{-1}\mathbf{A}$. Once the Cholesky factor had been computed, the equations were rewritten in two triangular systems, which were solved by simple forward and backward substitution. The actual computation was organised in the following steps:

(1) elimination of the attitude unknowns;

(2) Cholesky factorization of the (block partitioned) normal equations, solution of the equations by forward and backward substitution, and computation of the variances;

(3) solution of the attitude parameters, computation of the residuals to the observations, and testing of the solution.

The star part of the normal matrix was, even after elimination of the attitude parameters, very sparse (Figure 9.1). In the software only the non-zero elements of this matrix were stored and numerical operations were performed only on these elements. However,

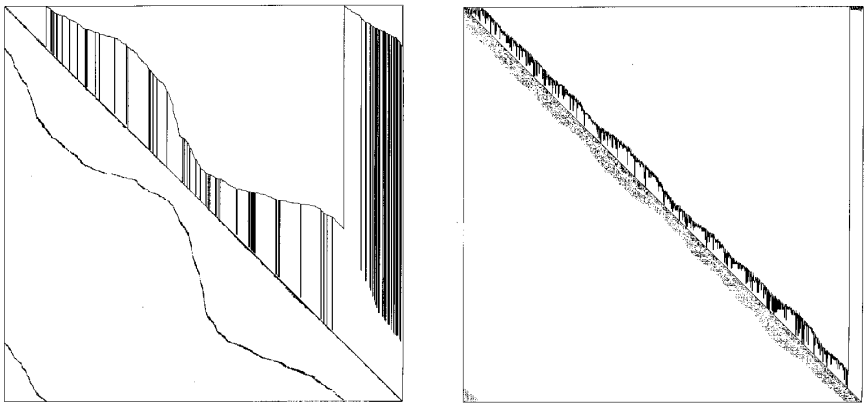

Figure 9.1. *Non-zero elements in the star part of the normal matrix (lower triangle) and envelope of the Cholesky factor (upper triangle) after elimination of the attitude parameters. The star parameters have not been re-ordered (left) or have been re-ordered by the modulo 60° algorithm (right) described by van der Marel (1988).*

during the Cholesky factorization new non-zero elements were created, causing so-called fill-in of the sparse matrix. The fill-in depended on the order in which the unknowns, and hence the rows and columns of the normal matrix, were given. Before the Cholesky factorization the star parameters were consequently re-ordered in such a way as to reduce the fill-in during the factorization (Figure 9.1). The reduction in computing time allowed by the re-ordering is considerable, not only for the factorization itself, but for all computations using it, such as the calculation of variances (van der Marel 1988).

The covariance matrix $\mathbf{Q}_{\hat{x}}$ of the least-squares estimator is the inverse of the normal matrix if $\mathbf{Q}_y^{-1}$ is used as weight matrix. The computation of the complete inverse would have been too time consuming and is also not very useful. However, a subset of the covariance matrix, corresponding to the non-zeroes in the Cholesky factor ('sparse inverse'), could be obtained in only twice the time of the factorization itself. The sparse inverse contained all the elements needed to perform statistical testing of the observations and to produce the proper diagnostics.

Slit Errors

The grid coordinates could be determined from the grid phase only up to an unknown integer number of slits. The slit numbers had to be computed from approximate values for the star and attitude parameters. Considering uncertainties in the *a priori* positions of 0.2 to 0.8 arcsec in the initial star catalogue, and the slit period of $\simeq$ 1.2 arcsec, it will be obvious that there were a substantial number of slit errors, resulting in ambiguities and inconsistencies throughout the first reduction iterations. The great-circle reduction suffered only from inconsistent slit numbers. It could not recognise a situation where all the grid coordinates of a certain star had the same slit error. Therefore, the computed star abscissae could still be wrong by one or more grid steps. The slit errors in the abscissae were ultimately corrected during the sphere solution and astrometric parameter extraction (see Section 11.6).

Slit inconsistencies resulted in contradictions between the observations of one star during the great-circle reduction. Several methods were used for detection and correction

of slit inconsistencies. First, inconsistencies in the linearized grid coordinates ΔG_{ik} per star were detected and corrected. This method works well when the attitude and instrument description were properly described. This method worked even better after improvement of the along-scan attitude, simultaneously by a sequential adjustment, using the grid coordinates ΔG_{ik} as observations and estimating correction to the along-scan attitude and star abscissa. It was possible that some slit inconsistencies were left at this stage. Therefore, after the least-squares adjustment the results were checked and remaining slit inconsistencies were corrected and a new solution was computed.

In further iterations of the great-circle reductions, the *a priori* values were taken from the last complete sphere solution, while NDAC also used at early reduction stages star coordinates determined from star mapper observations (see Chapters 6 and 7). In the final iterations of the great-circle reductions errors in the star catalogue used as input to the process were decreased to a level that slit number inconsistencies became very rare, and easy to correct when they occurred at all.

Statistical Tests and Validation

The results of the great-circle reduction were validated by statistical tests. On the basis of the outcome of these tests, in combination with internal and external iterations, several actions were possible:

(1) correction of slit numbers;

(2) skipping of doubtful observations, or (in NDAC only) re-weighting of observations;

(3) skipping stars from the normal equations solution (FAST passive stars).

Depending on the outcome of statistical tests, data was validated, i.e. accepted as sufficiently conforming to the model, or rejected (Section 9.7). In the latter case not only proper diagnostics were generated, but also a new solution without the rejected, and possibly erroneous, observations was computed. Two types of iterations were possible: external iterations of the complete great-circle reduction with an improved attitude description and star catalogue after a preliminary sphere solution and astrometric parameter extraction, and internal iterations within the great-circle reduction itself. Internal iterations mainly dealt with correction of slit inconsistencies and re-weighting of observations. Each iteration involved in principle a new least-squares adjustment. This was, of course, not a very attractive prospect. However, the burden was lightened considerably by *a priori* selection of suspected problem stars within FAST, combining internal iterations with necessary (for other reasons) external iterations, and special procedures for correcting slit inconsistencies.

The FAST great-circle reduction software did not distinguish between primary and non-primary reference stars, as was done in the sphere solution (Section 11.4), but rather between ‘active’ and ‘passive’ stars. Grid coordinates of active stars participated in the rigorous least-squares adjustment which computed the abscissae of active stars, along-scan attitude and instrumental parameters. The passive stars were added in later, using the previously computed active star abscissae, attitude and instrumental parameters, without changing them.

In general, passive stars were ‘problem’ stars, stars with a high probability of erroneous measurements, or very faint stars which did not contribute much to the attitude and instrumental solution. The passive stars were selected (by the software) by static criteria,

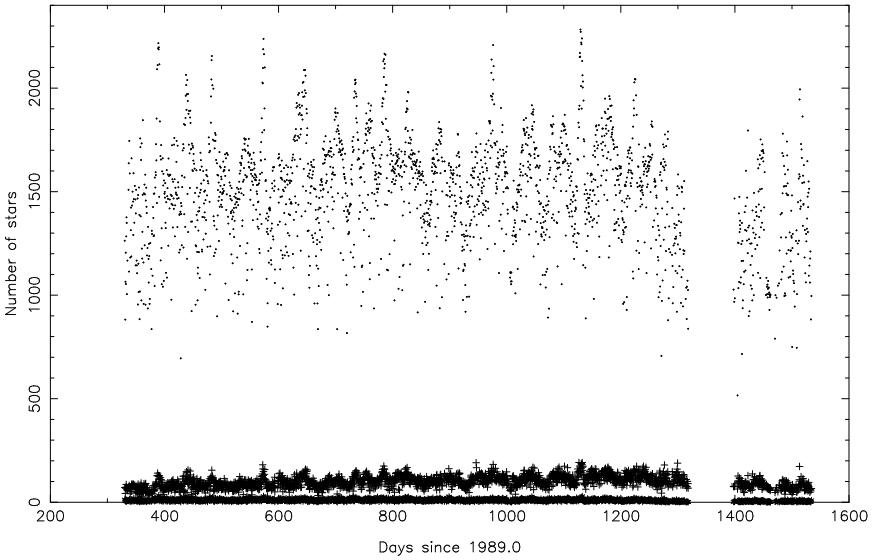

Figure 9.2. *Final number of active stars (dots), passive stars per reference great circle with 1-parameter solutions (+, the points just above the bottom of the graph) and 2-parameter solutions (×, the points at the bottom of the graph) during the mission (FAST).*

for example double star characteristics, as well as dynamically, based on the results of the statistical testing for star outliers (Equation 9.12). A few passive stars could only be computed if a linear motion—during the sets—was assumed (2-parameter solutions). As few as possible passive stars were selected during the last external iteration, to get the best possible precision for the star abscissae and attitude parameters. Therefore, during the procedure of external iterations, passive stars which turned out to have good solutions, were re-introduced as active stars during the next iteration. While, on the other hand, 'bad' active stars were treated as passive stars during the next iteration. On the average 300–400 passive stars were selected during the first treatment. In the final iteration this number was reduced to about 100. Figure 9.2 gives the final number of active and passive stars per reference great circle during the mission.

In the NDAC great-circle reductions data for identified 'problem' stars were not passed through this process, but were side-tracked to the special double-star processing (Chapter 13); thus all the stars retained for the great-circle reductions were effectively treated as 'active' stars.

9.3. Attitude Smoothing

The attitude of the Hipparcos spacecraft was, except for small vibrations (jitter) following thruster firings, a smooth function of time. Thus the along-scan attitude, which was initially computed once per observing frame of 2.133...s, could be further improved by introducing relations between the attitude values of neighbouring frames. In fact, an additional adjustment of the along-scan attitude, the so-called smoothing step, was carried out using a model for the attitude which required relatively few parameters.

The improvement of the attitude led also to improved star abscissae, and hence to an improved final star catalogue (Figure 9.3).

For attitude smoothing an additional equation was added to the observation equations for the geometric solution (Equation 9.5):

$$\mathbf{x}_A = \mathbf{B}\mathbf{x}_B \qquad [9.7]$$

The smoothed attitude could be expressed in a smaller number of parameters $\mathbf{x}_B$ than the frame-by-frame attitude $\mathbf{x}_A$ which was computed in the geometric solution step. The observation equations for the smoothed solution were:

$$\mathbf{y} = \mathbf{A}_A\mathbf{B}\mathbf{x}_B + \mathbf{A}_S\mathbf{x}_S + \mathbf{A}_I\mathbf{x}_I + \mathbf{e} \qquad [9.8]$$

The equations were again partitioned in an attitude, star, and instrument part, but now the star and attitude unknowns had changed roles: the stars were eliminated first, and the attitude unknowns—now much fewer than in the geometric mode—were re-ordered using the modulo 360° ordering (van der Marel 1988). In fact, the smoothed solution was computed as an update to the geometric solution. It was not necessary to re-compute the instrument parameters. They were already determined very well in the geometric solution. This was the approach in FAST. In NDAC a slightly different procedure was used: first Equation 9.5 was solved to give the geometrical attitude $\mathbf{x}_A$. This was then inserted in Equation 9.7, which was solved by least-squares to give the parameters $\mathbf{x}_B$ of the smoothed attitude. These, in turn, were inserted into Equation 9.8, together with $\mathbf{x}_I$ from the geometrical solution, and the resulting system was finally solved for the star parameters $\mathbf{x}_S$.

In the great-circle reductions the smoothed attitude was modelled by cubic B-splines. In general splines consist of polynomial segments, of fixed degree, joined end to end with continuity in a limited number of derivatives at the joints, the so-called knots. Actually, the B-spline series is a linear combination of shifted base functions or B-splines. It could represent the attitude at the milliarcsec level by choosing the right knots. This was performed automatically in the software. Thruster actuations were modelled as instantaneous impulses, which was justified in view of the relatively short duration of the pulses, which resulted in a discontinuity in the first derivative of the B-spline series at the thruster actuation time.

Smoothing of the attitude effectively increased the longitudinal field of view, since more stars were connected directly. Especially more bright stars were now linked directly to each other, and not only by chains of measurements between fainter stars (Lacroute 1983). Smoothing had, therefore, two favourable effects: it led to an overall increase in precision for the astrometric parameters and it permitted a more liberal observing strategy.

9.4. Rank Deficiency and Minimum Norm Solution

The observations in the great-circle reduction were invariant under a simultaneous shift of all the star abscissae v_i and all the along-scan attitude parameters ψ_k. This follows from the fact that the first two (dominant) terms in Equation 9.2 have practically equal and opposite coefficients. In practice this corresponded to an unknown zero point for the abscissae. The consequence was that the design and normal matrices in the great-circle reduction did not have full rank. Under normal circumstances the rank deficiency was

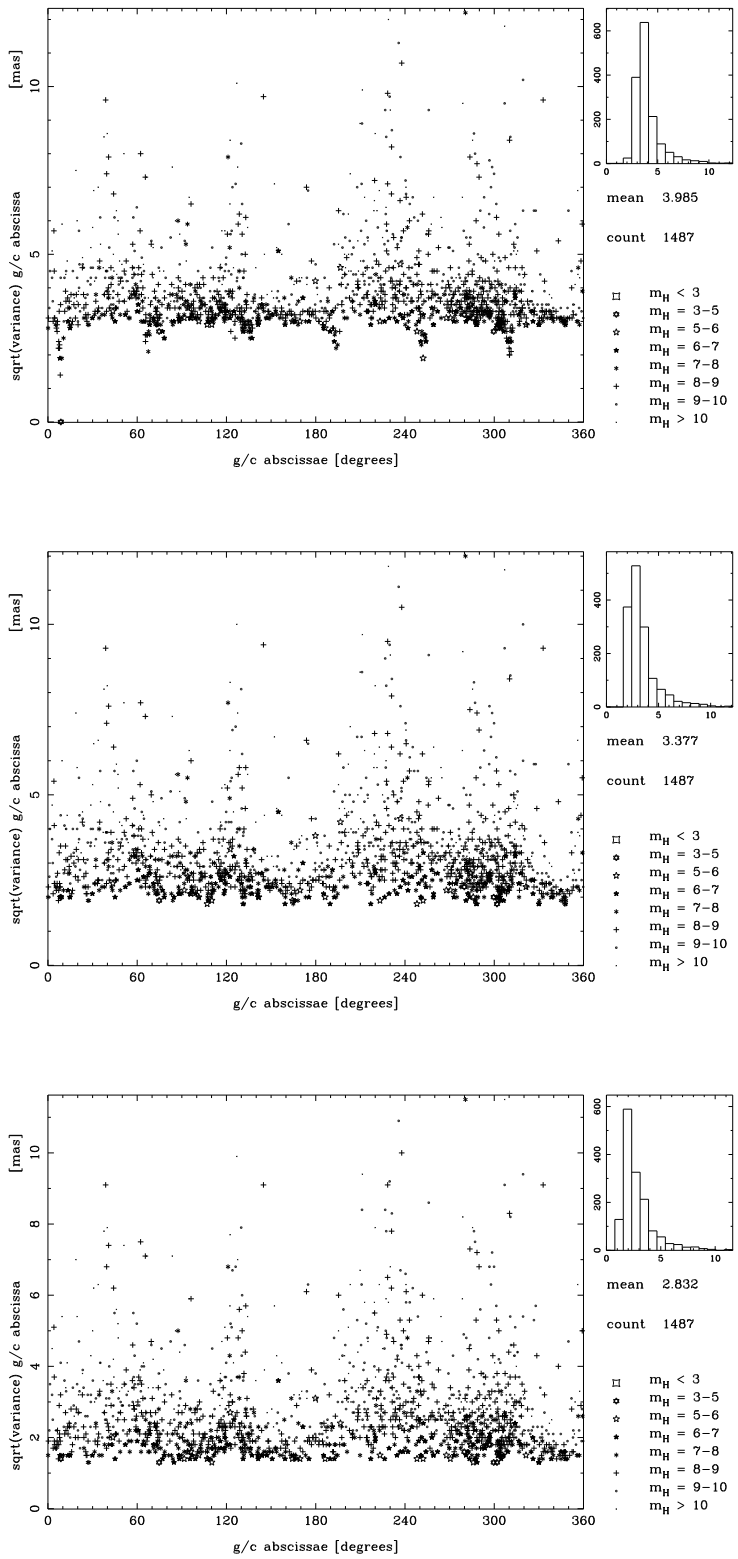

Figure 9.3. *Square root of the star variance versus the star abscissa for a base star solution (top), minimum norm solution (middle), and for the minimum norm solution after attitude smoothing (bottom). Data from 21 May 1990 10:00–17:20 (day 506).*

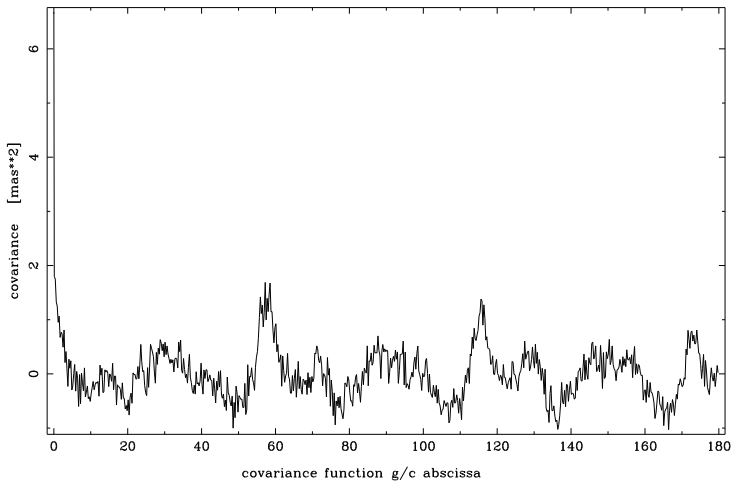

Figure 9.4. *Averaged auto-covariance function of the star abscissa (based on simulated data for the geometric solution).*

one. During the great-circle reduction the rank deficiency was provisionally eliminated by forcing the abscissa correction of one star, the so-called 'base star', to zero. This was equivalent to skipping the corresponding column in **A** and the corresponding row and column in the normal matrix. The base star was usually a bright star close to one of the scan circle nodes. This remedy for the rank deficiency was very attractive for its simplicity, but it resulted in a variance of zero for the base star (Figure 9.3). It had the same effect as adding the constraint equation $\mathbf{c}'\mathbf{x} = \mathbf{0}$ to the system, with **c** a vector of length n with all zeroes, except the element corresponding to the base star.

The choice of a particular base star was arbitrary, but it affected the solution and covariance matrix of the great-circle abscissae. For the sphere solution it did not matter which base star was chosen, if the full covariance matrix is used, because the unknown zero point was estimated anyhow. However, only the variances were taken into account for the weighting in the sphere solution, and, in this case, an arbitrary one of them was zero. This was not very satisfactory. Therefore, the great-circle solution and its covariance matrix were transformed into a minimum norm solution. The sum of the corrections to the star abscissa in the minimum norm solution were zero, the covariance matrix had minimum trace (minimum variance), there were no zero variances and off-diagonal elements in the minimum norm covariance matrix were smaller (Figure 9.3). Therefore, the minimum norm variances were preferred instead of the base star variances.

The minimum norm solution was computed from the base star solution by what is known in geodesy as an S-transform (Baarda 1973, Teunissen 1985). Again, the abscissae were only shifted, but from the original covariances the column and row average were subtracted, and the overall average was added. This operation was coded very efficiently during the Cholesky factorization. In fact, a constraint equation $\mathbf{c}'\mathbf{x} = \mathbf{0}$ was added to the equations, with **c** an n-vector with all ones, such that $\mathbf{Ac} = \mathbf{0}$, namely **c** is a basis for the null space of **A**.

The covariance matrix of the minimum norm solution was almost a cyclic matrix. A cyclic covariance matrix is fully described by a single covariance function. Figure 9.4 gives the averaged auto-covariance function of the star abscissae obtained from simulations for the nominal mission. The positive correlation between stars separated by a

basic angle (58°) and multiples are of course an effect of the two fields of view of the telescope. The basic angle was chosen not to be a fraction of 360° (see also Volume 2, Chapter 1, Figure 1.2). If the basic angle had been a fraction of 360° (for example 60°) the peaks would have been amplified. The value of 58° for the basic angle was the result of a study (in the mission design phase) on the great-circle rigidity. The correlation is larger for smaller data sets (which was the case in the revised mission). It was obvious that the correlations could not be neglected in the sphere solution without some loss of precision.

9.5. Accuracy of the Great-Circle Solution

The accuracy of the great-circle reduction depended first of all on the quality of the grid coordinates computed from the image dissector tube data. The standard error in the grid coordinates was dominated by the photon noise of the individual samples. The photon noise was Poisson distributed, but since each grid coordinate was computed from many samples one could assume, according to the central limit theorem, that the grid coordinates had a normal distribution and were uncorrelated with respect to each other. Thus the covariance matrix for the grid coordinates $\mathbf{Q}_y$, computed by the phase estimation task, was a simple diagonal covariance matrix. Other errors, like veiling-glare, projection and other modelling errors, which were smaller, were not represented by $\mathbf{Q}_y$ or by the covariance matrix $\mathbf{Q}_{\hat{x}}$ of the least-squares estimator. Therefore, the accuracy of the great-circle reduction could not be described by only the variances. Analysis of the residuals $\hat{\mathbf{e}}$ of the least-squares estimation by statistical tests, given in Section 9.7, was the other, very important, part of the accuracy description.

Both parts of the accuracy description were verified by tests on simulated data (van der Marel *et al.* 1989). Simulated data offered the possibility to study the error in the estimator, an advantage not available with real data. However, intercomparison of the results between FAST and NDAC gave another indication of the accuracy of the results. This was the third part of the accuracy description given in Section 9.8, and it was a very worthwhile one. In fact, creating the possibility of this kind of comparisons had been a major reason for assigning two consortia to the data reduction tasks.

Variance of the Star Abscissae

The variances of the star abscissae followed simply from the inverse of the normal matrix. The star variances were separated into three components:

(1) the variance σ^2_{obs} when only photon noise is taken into account, assuming a perfect attitude and instrument;

(2) the influence of the attitude determination σ^2_{att};

(3) the influence of the determination of the instrumental parameters σ^2_{ins}.

The variance of the star abscissae after adjustment was:

$$\sigma^2_{\text{star}} = \sigma^2_{\text{obs}} + \sigma^2_{\text{att}} + \sigma^2_{\text{ins}} \qquad [9.9]$$

The σ^2_{obs} of a star was computed from the cumulated *a priori* observation weights of this star and σ^2_{ins} was the difference of the computed star variances with and without solving

Table 9.1. Square root of the mean variances in milliarcsec per magnitude class (data from 21 May 1990 10:00–17:20 = day 506). The table shows the contributions of the observational errors (σ_{obs}), the instrument (σ_{ins}) and the attitude (σ_{att}) to the total standard error of the star abscissa (σ_{star}) for the geometric and smoothed solutions.

B (mag)	n_B	σ_{obs}	σ_{ins}	σ_{att} (geometric)	σ_{star} (geometric)	σ_{att} (smoothed)	σ_{star} (smoothed)
3–4	1	0.17	0.36	2.00	2.03	1.30	1.36
4–5	5	0.40	0.33	2.06	2.12	1.33	1.43
5–6	26	0.83	0.33	2.37	2.53	1.47	1.72
6–7	96	1.07	0.29	2.08	2.36	1.32	1.72
7–8	245	1.70	0.30	2.16	2.76	1.31	2.16
8–9	552	2.77	0.31	2.21	3.56	1.34	3.09
9–10	423	3.53	0.30	2.49	4.33	1.37	3.80
10–11	111	4.11	0.30	2.49	4.81	1.38	4.35
11–12	28	6.02	0.31	3.55	6.99	1.68	6.25
12–13	6	6.63	0.33	3.09	7.32	1.79	6.88
all	1493	3.01	0.30	2.34	3.82	1.36	3.31

for instrumental parameters. Finally σ_{att}^2 was a derived quantity, computed from the above mentioned variances.

In Table 9.1 the square root of the average of the minimum norm variance per magnitude class is given for the data set of Figure 9.3. The error σ_{obs}, and therefore σ_{star}, were clearly magnitude dependent: σ_{obs} varies between 0.1 mas for very bright stars and 3.2 mas for the 10 mag, and was even larger for 12–13 mag stars. The influence of the attitude and influence of the instrument were more or less the same for each magnitude class. The influence of the instrumental parameters (0.3 milliarcsec) was very small compared to the influence of the attitude. This value was very sensitive to the length of the reference great-circle set (Figure 9.13). It was a little larger than expected because the reference great-circle sets in the revised mission were shorter. The improvement brought by attitude smoothing is striking. The influence of the attitude was reduced very significantly (2.4 milliarcsec for the geometric solution and 1.4 milliarcsec in the smoothed solution), resulting in better star variances (Figure 9.3). The improvement affected the brighter stars in particular (Figure 9.5). The error in the fainter stars was still dominated by photon noise.

Attitude Smoothing

Figure 9.6 gives the variances of the attitude parameters for the example of Table 9.1. The differences between the geometric and smoothed attitude are shown in Figure 9.7. The influence of the attitude, σ_{att} in Equation 9.9, was reduced considerably by smoothing. The improvement was a function of the number of attitude parameters needed to represent the attitude. In Table 9.1 the mean standard error of the star abscissae was given for the optimum number of B-splines. In the unrealistic, but informative case of a perfectly known along-scan attitude, the standard error of the star abscissae is equal to σ_{obs} (neglecting the instrument).

The optimum number of B-splines was initially calculated by simulation experiments with the great-circle reduction software (van der Marel 1985). In Figure 9.8 the mean

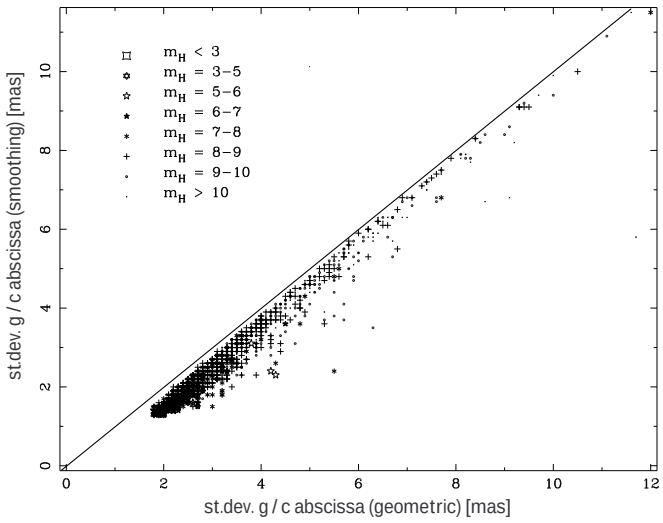

Figure 9.5. *Star abscissae improvement by attitude smoothing (data from 21 May 1990 = day 506).*

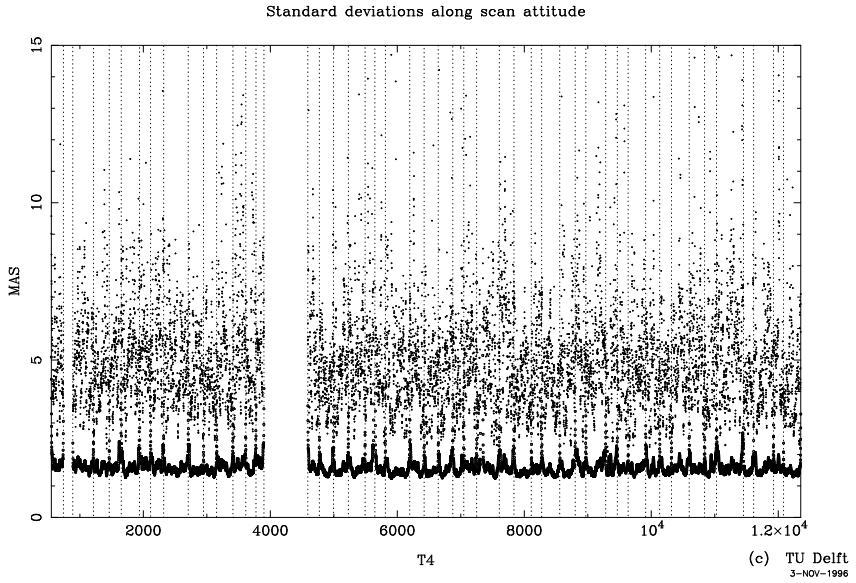

Figure 9.6. *Square root variance of the geometric (dots) and smoothed (circles, lower accumulation of symbols) attitude. Vertical lines are drawn at thruster actuation times. The time is given in units of $T_4 = 2.133\ldots$ s (data from 21 May 1990 = day 506).*

standard error (measurement induced error), the modelling error in the smoothed attitude, the rms error in the estimated attitude (estimation error) and the unit weight variance (Equation 9.10) are plotted versus the number of attitude parameters. The rms error in the estimated attitude and star abscissa reached a minimum at some point. With a smaller number of B-splines the modelling error became significant, for a larger number the inherent smoothness was not sufficiently exploited.

The rms errors in the estimated star abscissa could not be determined with real data. The only information available to determine the optimum number of B-splines with real data are statistical tests based on the test statistics in Equation 9.10–9.12, and on visual

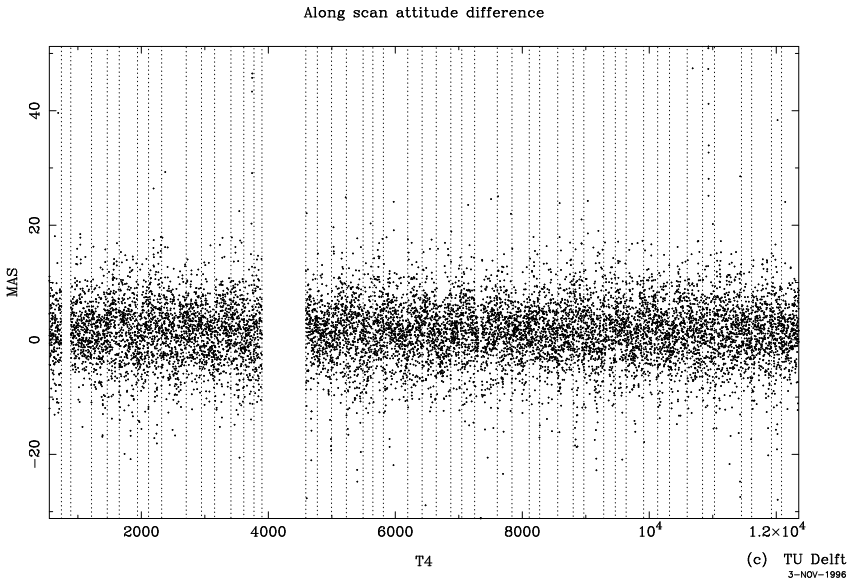

Figure 9.7. *Differences between the geometric and smoothed attitude (data from 21 May 1990 = day 506).*

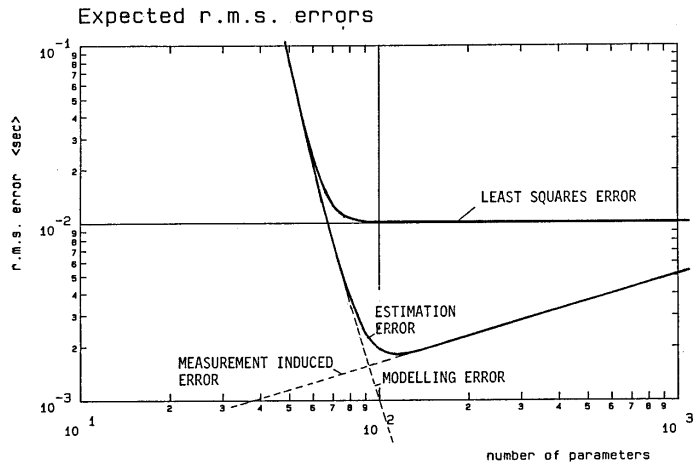

Figure 9.8. *Attitude improvement by smoothing as function of the number of attitude parameters per circle (based on simulations).*

inspection of the differences between the geometric and smoothed attitude for selected great-circle sets (Figure 9.7).

Figure 9.9 gives the square root of the average variance of the active star abscissae and the along-scan attitude during the mission. The improvement for the along-scan attitude by the attitude smoothing is striking. There is quite a significant number of great circles with a larger average standard error for the star abscissae and along-scan attitude. This is mostly for short great-circle sets, which had some difficulty in estimating the instrument parameters. This is also visible in the top plot of Figure 9.9, where the dots give the square root of the average of σ^2_{ins} of Equation 9.9.

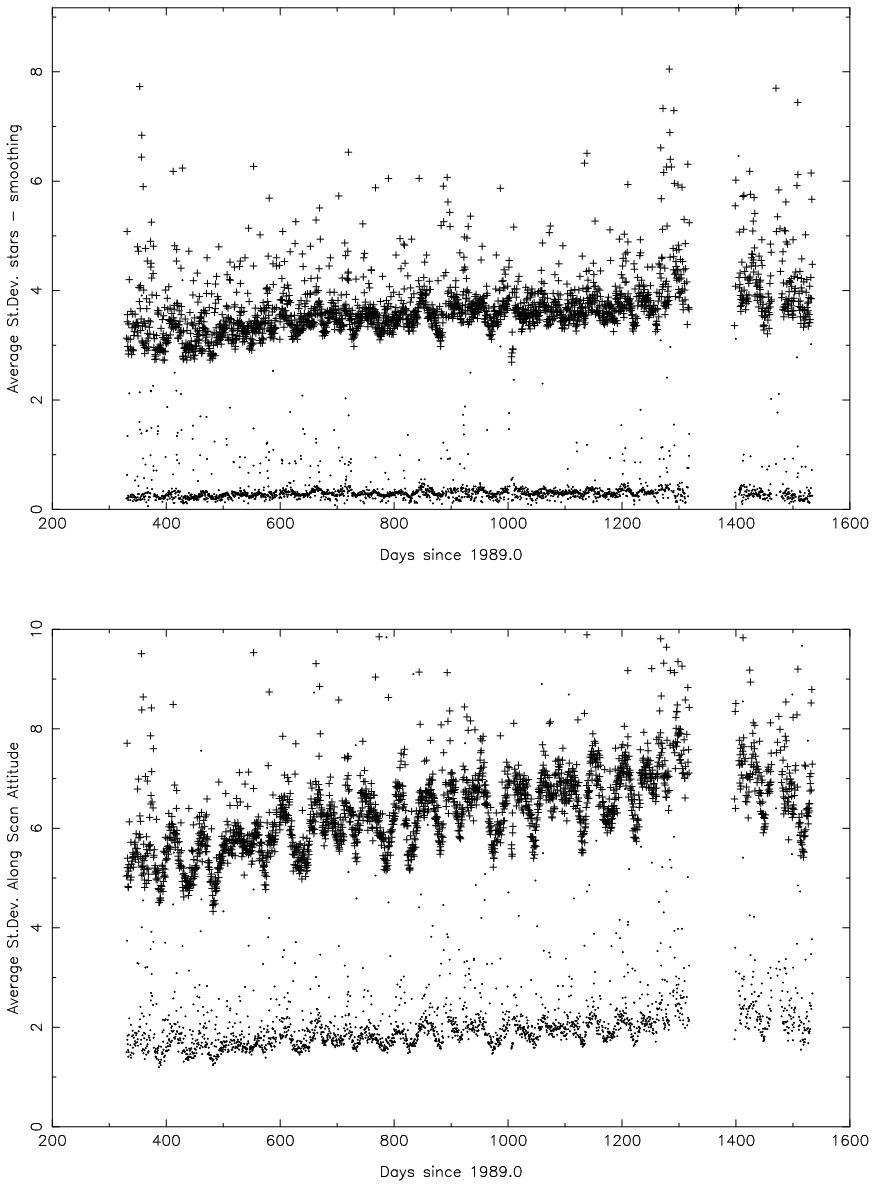

Figure 9.9. *Average standard error (square root of the average variance) in star abscissae after smoothing during the mission (top, crosses), influence of the solution of instrument parameters (top, dots), average standard error of along-scan attitude parameters (bottom) after smoothing (dots) and geometric (crosses) solutions during the mission.*

Projection Error

The projection error on the reference great circle, ϵ''_{ik} of Equation 9.4, depended on the size of the catalogue error Δr_i and star mapper attitude error $\Delta\theta_k$ and $\Delta\phi_k$. During the first treatment these quantities could be rather large due to the quality of existing star catalogues. Therefore, it was necessary to iterate the great-circle reduction after the sphere solution, making better values for r_i available. The attitude reconstruction was repeated too, resulting in better values for θ_k and ϕ_k. After at most two iterations the error in r_i was 2–4 mas and could be neglected, but the error in θ_k, ϕ_k remained of

Table 9.2. Predicted projection errors (in milliarcsec) during first treatment (assuming catalogue errors of σ_S = 1.5 arcsec) and in the iterations (assuming σ_A = 0.1 arcsec and negligible σ_S).

	First treatment		Iteration	
	rms	max	rms	max
Field coordinate	12.0	72.3	0.9	6.3
Attitude	6.0	72.3	0.8	6.3
Star	10.1	72.3	0.6	3.3

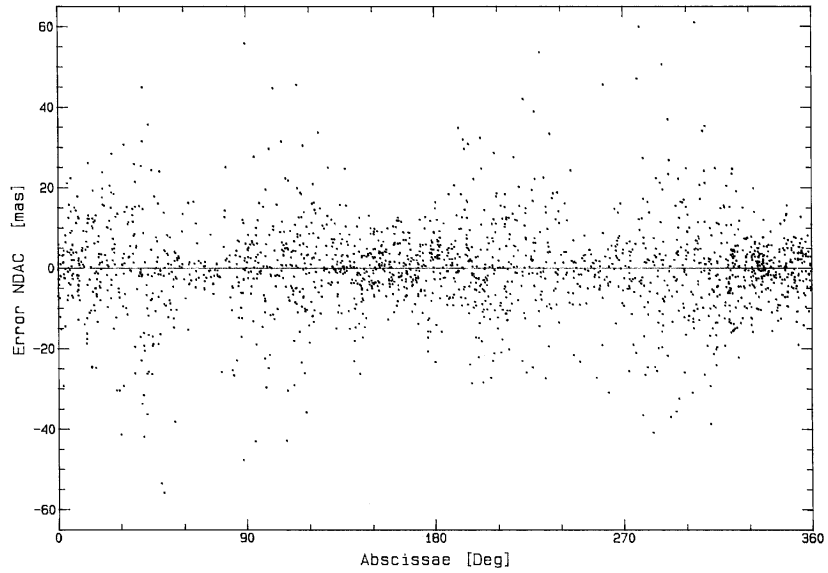

Figure 9.10. *Projection error in the star abscissae. The nodes are near 70° and 250°*

the order of 50–100 mas, due to star mapper photon noise, and could not be improved further.

In Table 9.2 the projection error effect on the field coordinates, star abscissa and along-scan attitude are given for a typical reference great circle. The results are from analytic formulae, and were confirmed by extensive simulations (van der Marel 1988). The projection error depended also on the size of the partial derivatives. The projection errors were large when the inclination of the scanning direction with respect to the reference great circle was large. Therefore the projection errors were large near the nodes of the scan circles. However, the projection error effect on the attitude and star parameters averaged out at locations with a uniform scanning. This happened exactly on the nodes of the scan circles. Therefore maximum projection errors were expected near the nodes, but not on the nodes. Figure 9.10 is a scatter diagram of the projection error effect on the star abscissae for a typical first treatment. The predicted maxima near the nodes are clearly visible.

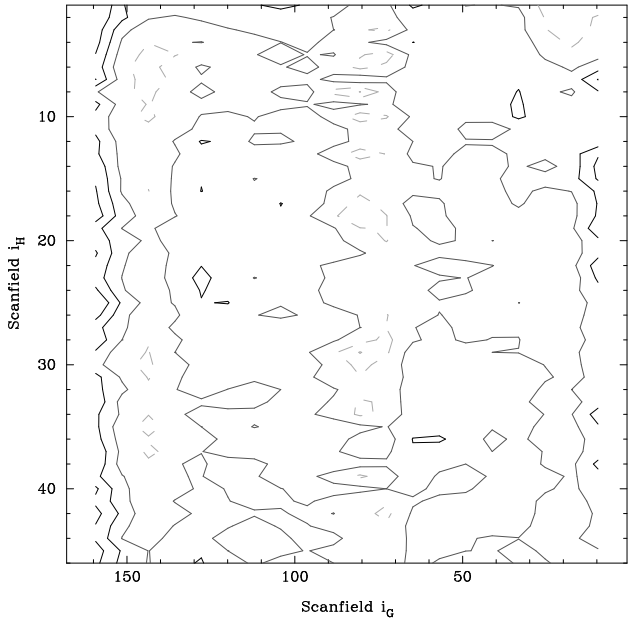

Figure 9.11. *Medium-scale residuals of a third degree polynomial representation of the non-chromatic field-to-grid transformation. The contours range from +1 mas (solid line) to −0.5 mas (broken, dotted line). See also Figures 10.14 to 10.16.*

9.6. Instrument Parameters

The basic angle distortion and large-scale field-to-grid transformation is the third group of parameters which was estimated during the great-circle reduction. The field-to-grid transformation was modelled by a polynomial in several variables. The polynomial degree was 3 or 4 for the non-chromatic terms and 1 for the chromatic terms. Figure 9.11 shows a grid map of the mean residuals over the first 30 months of reduced data, where third or fourth degree polynomials were adopted to describe the non-chromatic part of the field-to-grid transformation.

A new set of instrument parameters was normally estimated for each great-circle reduction. However, since the highest order parameters were assumed not to change with time, these parameters were fixed at their average values. The choice and time evolution of the instrument parameters is described in more detail in Chapter 10 and in Volume 2, Chapter 10. Here some of the implementation aspects are described briefly.

The choice for a power series was a little arbitrary. At the time of implementation there were no numerical or functional reasons for choosing different types of functions. However, there were signs from the real data that some refinements were necessary. A disadvantage of power series was certainly the large correlation between some of the estimated parameters. In any case, not all of the instrumental parameters can be estimated equally well. The so-called 'constant term' (g_{00} in the NDAC notation), and the 'constant chromaticity' (c_{00}), could not be estimated at all from a single reference great-circle set. They were omitted from the great-circle equations and determined during the sphere solution (see Chapters 11 and 16).

In FAST, it was shown that the variances of stars and attitude determinations could be improved when less instrumental parameters were taken as unknown and replaced by fixed pre-determined values. These were obtained by computing the mean of the coefficients determined by the great-circle reduction during earlier iterations for every calibration period as defined in Section 4.2. In addition, the variations of the basic angle were modelled by a linear function of time. The analysis of the instrumental parameters showed that a fourth-order polynomial gave a significantly better representation of the field-to-grid transformation as shown in Figure 9.11, and that the third and fourth degree terms were very stable throughout the mission, but were rather strongly correlated with certain first and second degree terms.

From these considerations, the following scheme was adopted by FAST. While the first treatment of data was performed using third-order polynomials, the next iteration was performed with fourth-order formulae. Then, in further iterations, the calibrated third and fourth degree coefficients as well as the chromatic terms were considered as known, reducing by 11 the number of instrumental unknowns. For short reference great circles (1 or 2 rotations), the terms proportional to y, xy and y^2 (where x is along the scan and y normal to it) were difficult to estimate because the inclination was small, the risk being large variances for star parameters and even a singular system of equations. They were then taken from the calibration file. In case of even shorter data sets, no instrumental parameters were computed except the coefficients for x and x^2; all the others, including the basic angle, being taken from the calibration. Finally, when thermal disturbances occurred (see Chapter 2), the basic angle was not stable and its variations were represented by a linear function of time.

Figure 9.12 gives the number of instrument parameters which were solved by the FAST consortium during the final iterations as a function of the length of the great-circle set. Also plotted are the average standard error of the stars and the influence the instrument parameter estimation had on the standard error of the stars. In shorter great-circle sets less instrument parameters were solved than in longer sets. For the longer sets, which had the power to estimate the more difficult instrument parameters, fewer instrument parameters were replaced by values taken from the calibration. Even despite this strategy, the effect of the instrument parameter solution on the standard error of the star abscissae was more pronounced for the shorter reference great-circle sets.

9.7. Analysis of the Least-Squares Residuals

The least-squares adjustment can be interpreted as the orthogonal projection of the m dimensional vector of observations $\mathbf{y}$ ($\in \mathbb{R}^m$) onto the vector $\hat{\mathbf{y}} = \mathbf{A}\,\hat{\mathbf{x}}$ in the n dimensional linear manifold spanned by the columns of $\mathbf{A}$ (the range space). The metric of $\mathbb{R}^m$ is defined by the weight matrix $\mathbf{Q}_y^{-1}$ of the observations (which is in fact a metric tensor). The adjusted observations $\hat{\mathbf{y}}$ and least-squares residuals $\hat{\mathbf{e}}$ are orthogonal, so the residual sum of squares $E = \hat{\mathbf{e}}'\mathbf{Q}_y^{-1}\hat{\mathbf{e}}$ is a minimum. Moreover, the residual sum of squares has a χ^2 distribution with $m - n$ degrees of freedom if $\mathbf{y}$ has a normal distribution with $N(\mathbf{Ax}, \mathbf{Q}_y)$. Dividing E by the degrees of freedom leads to the Fisher test statistic with $m - n$ and ∞ degrees of freedom, or unit weight variance:

$$F = \frac{E}{m-n} = \frac{1}{m-n}\sum_i \sum_k \frac{e_{ik}^2}{\sigma_{ik}^2} \simeq F(m-n, \infty) \qquad [9.10]$$

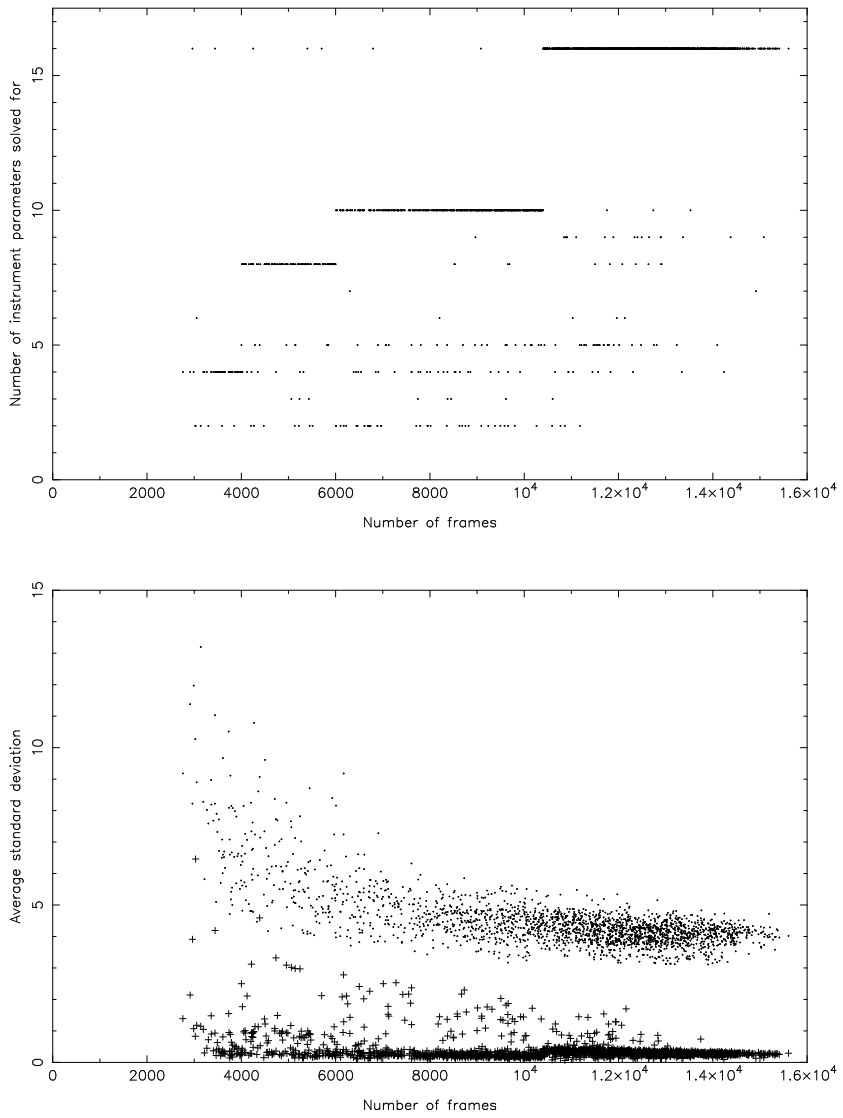

Figure 9.12. *Number of instrument parameters solved during the final iterations versus the length of the great-circle sets (top), and the average standard error of the stars (dots) and the influence of the instrument* σ_{ins} *(+) as a function of the length of the great-circle sets (bottom).*

with e_{ik} the least-squares residual of star i in frame k and σ_{ik} the standard error of the observation. The expected value of F is one. The null hypothesis H_0 that the model of Equations 9.5 and 9.7 and covariance matrix $\mathbf{Q}_y$ were correct, and there were no outliers, was verified by hypothesis testing. The test was:

$$\text{reject H}_0 \text{ if } \quad F > F_\alpha(m-n, \infty) \qquad [9.11]$$

with $F_\alpha(m-n, \infty)$ the critical value for the test with level of significance α, the probability that the test was rejected wrongly if H_0 was true.

Figure 9.13 gives the value of F during the mission. The values for F were larger for smoothing. Almost every value for the smoothed solution exceeded the expected value of 1 significantly, resulting in a rejection of the test in Equation 9.11. For a typical reference great-circle set the critical value was $F_{0.001}(20\,000, \infty) = 1.03$. The rejections were a result of the modelling error in the attitude. The B-spline series was only able to

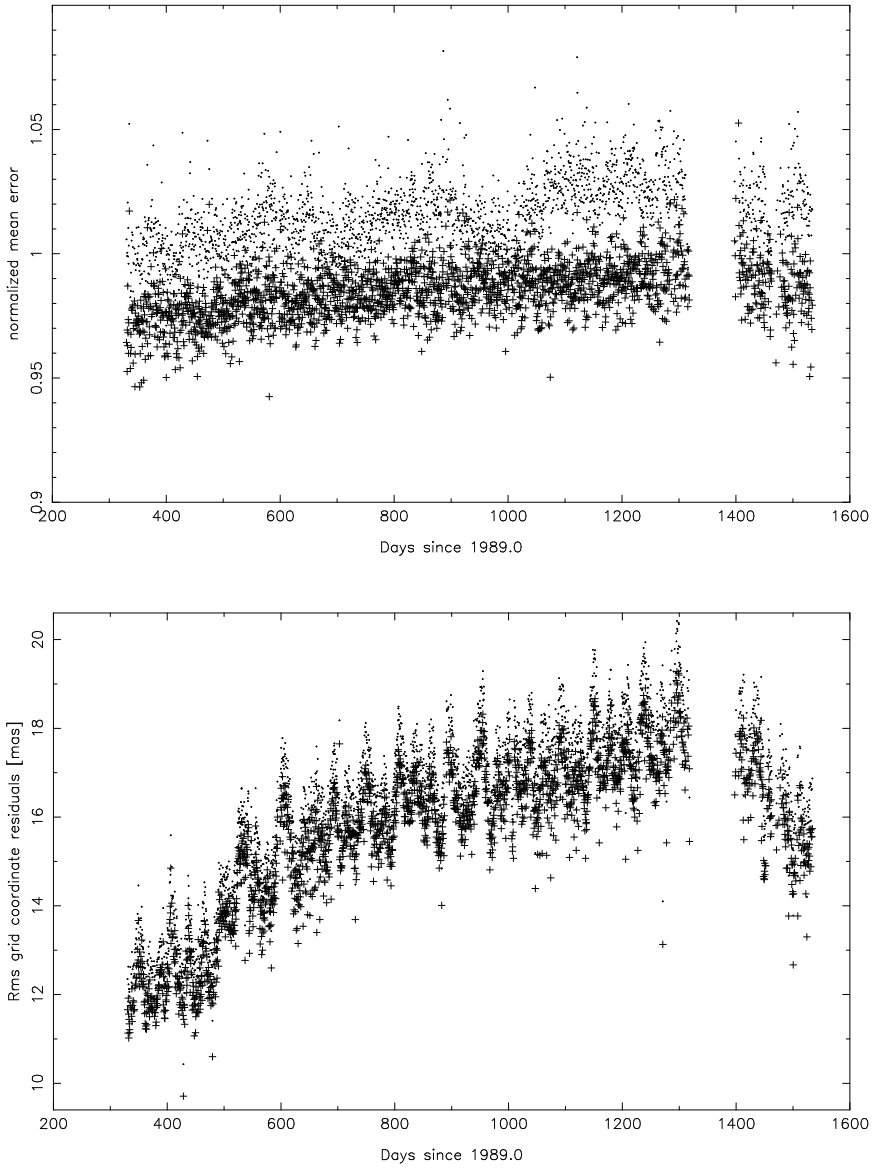

Figure 9.13. *Unit weight variance F (top) and rms error of the residuals of the grid coordinates (bottom) during the mission (crosses refer to the geometric solution, dots to smoothing).*

describe the attitude up to the 1 milliarcsec level. Taking these into account, the tests were almost always accepted. Despite all this the F test values were close to one. This meant that the variances of Table 9.1 were representative. For this particular data set the F test values were 1.048 and 1.076 respectively for the first treatment, and 0.9688 and 0.9974 for the final iteration given in Figure 9.13.

The power of the test in Equation 9.11 was not very good. A few small errors in the observations did necessarily lead to a rejection of this test. Neither did it provide an indication of what problems caused rejection. Fortunately other more powerful tests

could be used to identify specific problems. The quality of the adjusted star abscissae was checked by a Fisher test statistic similar to Equation 9.10:

$$F_i = \frac{1}{s_i} \sum_k \frac{e_{ik}^2}{\sigma_{ik}^2} \quad \text{with} \quad s_i = \sum_k \frac{\sigma_{e_{ik}}^2}{\sigma_{ik}^2} \qquad [9.12]$$

with s_i the degree of freedom, or redundancy, of star i, computed from the variance of the least-squares residuals $\sigma_{e_{ik}}^2$. F_i has a Fisher distribution with s_i and ∞ degrees of freedom, which could be used in the test of Equation 9.11. Also used was F_i/F instead of F_i. F_i/F has a Fisher distribution with s_i and $m-n$ degrees of freedom. This test was indicative of modelling problems related to specific stars, e.g. single stars which turned out to be double, veiling-glare, etc.

The star-by-star test was the main instrument for the selection of FAST active and passive stars. The static criteria which were applied during the first treatment were gradually replaced by the results of this test. After every external iteration the results of the star-by-star test from all great-circle sets participating in the iteration were collected. Those stars which had many rejections during the great-circle treatment were then selected as passive stars for all great-circle sets in the next iteration. Passive stars which had very few rejections, were selected as active stars for the next iteration. In addition to the global list of active and passive stars, another list was maintained in which stars were made passive for specific great-circle sets. In this way, an occasional star outlier could be accommodated. During the first treatment about 300 to 400 passive stars per great-circle set were selected using static criteria, and up to 2 per cent of *a priori* unsuspected active stars were flagged. In the final iteration, about 100 passive stars per set were left (Figure 9.2), and there were no serious rejections of the test of Equation 9.12.

Statistical tests similar to Equation 9.12 were derived to specifically check the frame-by-frame attitude and B-spline smoothing by altering the summation in Equation 9.12. The test on the B-spline intervals was indicative of the modelling error in the smoothed attitude caused by insufficient B-spline parameters. This test was used within FAST to build a list of intervals which needed additional B-spline parameters, or should be excluded from the reductions completely, for instance because the satellite had been hit by small particles, or for other reasons. Some periods had so many new B-splines that effectively a frame-by-frame attitude representation was used. Although this procedure was automated by FAST to some extent, manual intervention was necessary on several occasions. The advantage of using a list was that this work did not have to be repeated in subsequent iterations.

The summation in the test of Equation 9.12 could be restricted to a single observation, which resulted in the test statistics with standard normal distribution:

$$\bar{e}_{ik} = \frac{e_{ik}}{\sigma_{e_{ik}}} \sim N(0,1) \qquad [9.13]$$

A grid coordinate error was suspected if $|\bar{e}_{ik}| > N_\alpha(0,1)$. Using this test the grid coordinates were inspected one by one. This procedure is a common technique in geodesy and is known as 'data snooping' (Baarda 1968). The major problem with these techniques was a lack of robustness caused by smearing and masking effects. Smearing was caused by the correlation between the least-squares residuals. A single outlier in the data could result in the rejection of several data snooping hypotheses. Similarly, a large outlier may mask smaller outliers, which could only be found after the large outlier had been removed. Therefore, whatever the procedure for detection and correction was, it had to be iterated: i.e. the most evident cases were tackled first, then a new solution

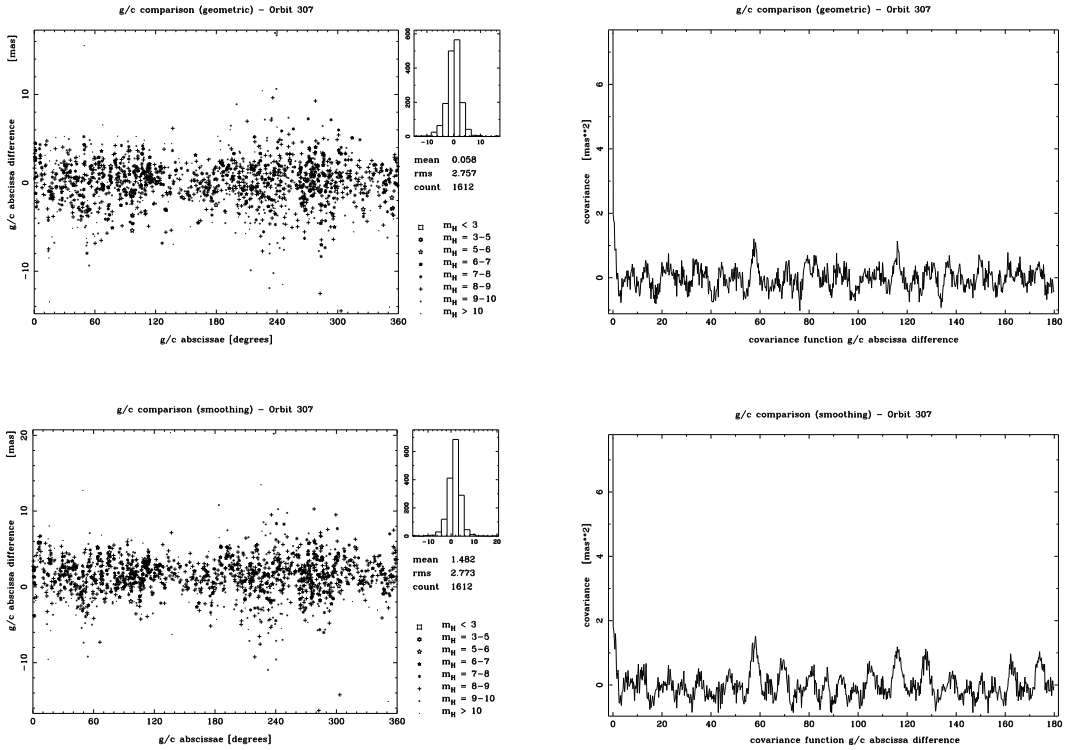

Figure 9.14. *Intercomparison of the FAST and NDAC abscissae after attitude smoothing (data from 14 May 1990 0:04–5:08 = day 499).*

was computed and the residuals, or testing variates, were inspected again. The process converged if in later iterations more and more subtle cases were recognised as errors. This procedure can be automated. This was for instance implemented by Kok (1985) in his iterated data snooping procedure, or by Eeg (1986) in his iteratively re-weighted least-squares, which was the method used by NDAC.

9.8. Intercomparisons

Several identical sets were reduced by NDAC and FAST for comparison purposes. Figure 9.14 shows the difference in abscissae for a typical comparison set halfway during the reductions, just after the input catalogue had been improved for the first time. Passive stars, which had differences up to several hundred milliarcsec, were removed from Figure 9.14. These differences were caused by the different treatment of double stars in the two consortia. In the FAST great-circle reduction the weighed mean of the first and second harmonic of the grid phase were used as the observation. In NDAC only the first harmonic was used (see Chapter 5). This affected the double stars in particular.

The comparison set shown in Figure 9.14 is one of 15 comparison sets—with specific difficulties—which were tested during the mission. The difficulty with the set in Figure 9.14 was an eclipse, but this had no adverse effects in this case. Actually, this comparison set was an example of a normal set. Other comparison sets sometimes

Table 9.3. Summary of projection error differences resulting from the use of different star catalogues for the NDAC great-circle reduction. All values are given in milliarcsec. The rms errors for the two catalogues were 270 milliarcsec (Hipparcos Input Catalogue) and 185 milliarcsec (partially improved working catalogue).

	Abscissa			Instrument
	rms	min	max	(corner)
Set 1 (all stars)	2.68	–40	+25	0.3
Set 1 (active stars)	1.56	–25	+8	0.5
Set 2 (all stars)	2.94	–70	+10	0.4

had much larger differences, with large systematic effects. Often a very significant 6th harmonic was found, which was due to the basic-angle design, one of the periods for which the great circle was not very robust. This 6th harmonic could be triggered by almost anything, for example a serious outlier in the data, or short great-circle sets in combination with estimating too many instrument parameters. Also in good comparison sets this harmonic was present, as can be observed from the averaged auto-covariance function in Figure 9.14. This led to experiments in the sphere solution (Chapters 11 and 16) whereby it was tried to estimate a 6th harmonic for each great-circle set.

The rms difference for good comparison sets was usually 3–5 milliarcsec, with maximum errors up to several tens of milliarcsec. The rms differences seemed to be too large considering that both consortia had reduced the same data. The rms difference was of the same order as the standard error of the star abscissae. Also, the correlation between the abscissa differences, given in Figure 9.14, was very similar to the correlation function of the great-circle abscissae in Figure 9.4 (computed from simulated data). In fact, two completely independent measurements would have resulted in differences which were not much larger. This requires some explanation. The first reason was that the consortia did not really use the same data because NDAC did not use the second harmonic of the grid phase. This mainly affected the double and multiple stars. There was a variable bias between the first and second harmonic which also affected the single stars and especially the calibration of the instrument (Schrijver & van der Marel 1992).

The second reason was that the projection errors were not the same because different working catalogues and star mapper attitudes had been used. The rms difference in the star catalogue used for this particular example was 0.1–0.3 arcsec. The effect was illustrated by comparing two runs of the same consortium on the same data with different catalogues, but otherwise completely identical. The results are given in Table 9.3. An error in a single catalogue position would also affect the other stars due to the smearing effect of the least-squares estimation. The covariance function was, therefore, similar to the covariance function of the abscissae.

The third reason was that different sets of observations and stars participated in the actual least-squares adjustment. In FAST the so-called passive stars were fitted in later without affecting the attitude. Outliers in the observations were treated differently. In NDAC the great-circle reduction was iterated several times with some of the observations re-weighted. FAST used data snooping for the grid coordinates and variance tests for the stars. When an active star was rejected by the statistical tests it was made passive in the next external iteration. The effect of using passive stars was studied by two runs on the same data with different sets of stars. The results are given in Table 9.4. A fourth reason is that in the attitude smoothing the number of B-splines and the location of their

Table 9.4. Effect on the abscissa differences when different sets of stars were selected (FAST active star set versus all stars). All values are given in millarcsec.

	Abscissa			Instrument
	rms	min	max	(corner)
NDAC	2.32	–42	+10	0.4
FAST (geometric)	1.99	–10	+9	0.3
FAST (smoothing)	1.56	–5	+5	–

Table 9.5. Normalised standard errors for great-circle reductions with weighted phase, first harmonic and second harmonic only.

	Weighted	First only	Second only
Geometric solution	1.019	1.017	1.030
Smoothed solution	1.043	1.040	1.043

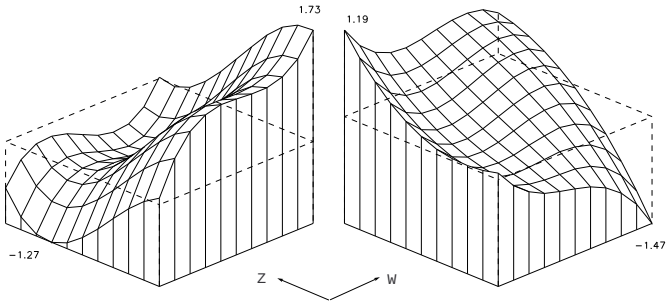

Figure 9.15. *Difference between the FAST and NDAC instrument description (first harmonic).*

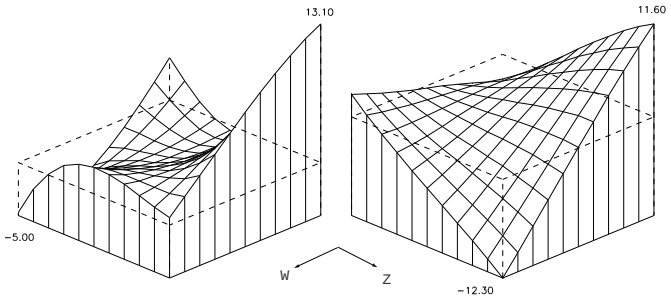

Figure 9.16. *Difference between the instrument for the first harmonic and second harmonic.*

knots were different. Also, the estimation procedures in FAST and NDAC were not the same.

The instrument parameters agreed up to 1.5 mas in the corners of the field of view when FAST used the first harmonic of the grid phase. The only significant differences, i.e. more than two times the standard error, were in the terms g_{01} and g_{30} (+1.4 and −0.94 mas, respectively, at the upper left corner of the field of view, see also Figure 9.15). When FAST used the weighted phase, which was their standard approach, the agreement was lost between the FAST and NDAC instrument parameters. This did not mean that the weighted phase is worse, it only meant that the field-to-grid transformation was different. In fact, test runs with only the second harmonic showed that it is good data (Table 9.5). The difference in instrument parameters for the first and second harmonic are shown in Figure 9.16. The differences in the corners were 13 mas.

9.9. Conclusions

In the previous sections results of the great-circle reductions have been given based on simulations, comparisons, or the software's internal accuracy description. The accuracy of the software's internal accuracy description has been verified in every possible way. A final test was the next reduction step: the sphere solution. Here the abscissae from the great-circle reduction with their minimum-norm standard error were used as observations. Statistical tests, like those in Equation 9.12, were used to verify the abscissae observations and the stochastic model. Considering the fact that at the level of the sphere solution abscissae from the same great-circle set were assumed to be uncorrelated, which they were not (Figure 9.4), it turned out that the great-circle software gave a very fair description of the accuracy.

H. van der Marel, F. van Leeuwen, J. Kovalevsky, C. Petersen